Polymer 311 (2024) 127574

Contents lists available at ScienceDirect

Polymer

journal homepage: www.elsevier.com/locate/polymer

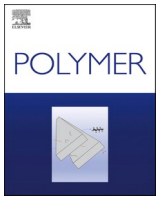

Design and mediated hydrogen bonding strength of Poly(styrene-*alt*- *N*–(ethyl–4–hydroxyphenyl)maleimide) copolymer to enhance miscibility with hydrogen bonded acceptor homopolymers

Tzu-Ling Ma, Wei-Ting Du, Shiao-Wei Kuo *

Department of Materials and Optoelectronic Science, Center for Functional Polymers and Supramolecular Materials, National Sun Yat-Sen University, Kaohsiung, 804, Taiwan

ARTICLE INFO

Keywords:
Hydrogen bonding
Miscibility
Tyramine
Thermal property
and 2D-FTIR

ABSTRACT

In this study, the monomer *N*–(ethyl–4–hydroxyphenyl)maleimide (TyHPMI) was synthesized from tyramine and maleic anhydride. Subsequently, free radical copolymerization was used to prepare the poly(S–*alt*–TyHPMI) alternating copolymer by reacting TyHPMI with styrene. We confirmed the chemical structure using Fourier transform infrared (FTIR), ^{1}H and ^{13}C nuclear magnetic resonance (NMR). The sequence distribution of the poly (S–*alt*–TyHPMI) alternating copolymer was analyzed using mass–analyzed laser desorption ionization/time–of–flight (MALDI–TOF) mass spectrometry. Differential scanning calorimetry (DSC) measurements showed a single glass transition temperature (T_g) across various weight fractions of binary blended systems containing strong hydrogen–bonded acceptors, such as poly(S–*alt*–TyHPMI)/poly(4–vinyl pyridine) (P4VP) and poly(vinyl pyrrolidone) PVP, implying full miscibility. The T_g values predicted by kwei equation for the poly (S–*alt*–TyHPMI)/P4VP and poly(S–*alt*–TyHPMI)/PVP blends show a positive deviation from linearity. This deviation is due to the short alkyl chain reinforcing the addition of acidic TyHPMI units, which enhances intermolecular hydrogen bonding between the pyridyl or C=O groups and the OH units of the TyHPMI segment. As a result, FTIR spectral analyses indicate that the intermolecular hydrogen bonding between pyridyl and C=O groups is stronger in the poly(S–*alt*–TyHPMI) copolymer compared to the poly(S–*alt*–HPMI) copolymer. This is supported by the larger ratio of the inter/self-association equilibrium constant (K_A/K_B) value.

1. Introduction

Polymer blends are materials formed by physically mixing two or more different polymers, resulting in a new material with improved mechanical, thermal, and morphological properties [1–5]. Among these properties, the miscibility of the polymers in the blend plays a crucial role, significantly influencing the overall performance. Flory–Huggins lattice theory described the thermodynamics of polymer blends, highlighting that factors such as high molecular weight and polymer solubility often result in phase separation and poor performance. To overcome these problems, Painter and Coleman proposed that introducing specific interactions, hydrogen bonding, could effectively reduce the Gibbs free energy in the Flory-Huggins equation [6,7]. Based on the Painter–Coleman association model [6,7], the miscibility of these polymer blends was determined by the hydrogen bond equilibrium constant ratio K_A/K_B (inter–associated/self–associated). Several factors impact the K_A/K_B ratio, including the basicity of the hydrogen bond acceptor, the acidity of the hydrogen bond donor, sequence distribution causing intramolecular screening effect and the accessibility of hydrogen bonded functional groups, steric effects, and environmental conditions such as temperature and solvent [8–13].

In our group during last two decades, we extended the research of hydrogen bonding in polymer blends for further applications by adjusting the K_A/K_B ratio. For example, poly(ethylene oxide) (PEO) and polycaprolactone (PCL) have value of K_A = 280 and 90 when blending with PVPh with value of K_B = 66.8 [7,8]. By leveraging the difference in the hydrogen bonding acceptor strength (K_A) between PEO and PCL, these polymers could be combined to form PEO–*b*–PCL based diblock or triblock copolymers. When these copolymers were blended with phenolic OH units, the stronger hydrogen–bonded acceptor properties of PEO induce microphase separation. A variety of nanostructures can be produced by fine–tuning the proportions of each component in the blend

* Corresponding author.
E-mail address: kuosw@faculty.nsysu.edu.tw (S.-W. Kuo).

https://doi.org/10.1016/j.polymer.2024.127574
Received 20 July 2024; Received in revised form 19 August 2024; Accepted 1 September 2024
Available online 1 September 2024

system. Subsequent thermal pyrolysis or carbonization of these nanostructures yields self–organized mesoporous materials. These materials hold potential applications in areas such as CO_2 adsorption and energy storage [14–21]. There were also examples include PEO–*b*–P4VP, PEO–*b*–PLA, PCL-*b*-P4VP, and PEO–*b*–PCHC [20–25].

Among hydrogen bonding polymer blends, the studies of alternating copolymers have been rarely explored. Recently, we began investigating hydroxyphenylmaleimide (HPMI) derivatives and copolymerizing them with styrene to achieve near–perfect alternating copolymers, PS–*alt*–PHPMIs, based on the Mayo–Lewis equation [26]. To explore the miscibility in a series of PS–*alt*–PHPMIs, we conducted experiments blending these copolymers with stronger hydrogen–bonded acceptors such as PVP or P4VP [27,28]. However, according to the Kwei equation [29], the poly(S–*alt*–HPMI)/P4VP binary blends exhibited a negative value of *q*. This is because the inter–associated hydrogen bonding between poly(S–*alt*–HPMI) and P4VP is weaker than the self–associated hydrogen bonding within poly(S–*alt*–HPMI) ($K_A < K_B$). Leveraging this weak inter–associated hydrogen bonding, we placed our poly(S–*alt*–HPMI)/P4VP binary blending system into a selective solvent for pursuing potential applications in micelle formation successfully [30,31].

To further develop our micelle system, in this study, we developed a new series of HPMI derivatives by reacting maleic anhydride with a bio-based material, tyramine, which is widely used in biological applications and demonstrates excellent thermal and mechanical properties [32–34]. Subsequently, we utilized conventional free radical copolymerization again. This allowed us to synthesize the poly(S–*alt*–TyHPMI) alternating copolymer by reacting TyHPMI with styrene. Compared with HPMI units in poly(S–*alt*–HPMI), the TyHPMI units feature an additional two short alkyl units, which could strongly reduce the intramolecular hydrogen bonding of phenolic OH units with C=O units of HPMI segment. As a result, we could expect that the intermolecular hydrogen bonding of TyHPMI segment with P4VP or PVP homopolymer because of the increasing K_A/K_B ratios. We investigated the miscibility of poly(S–*alt*–TyHPMI) by blending with P4VP or PVP homopolymer. The chemical structure of the resulting poly(S–*alt*–TyHPMI) was verified using FTIR, ^{1}H and ^{13}C NMR spectroscopy. The alternating sequence distribution was assessed using MALDI–TOF mass spectrometry. DSC thermal analyses provided evidence that the full miscibility of poly(S–*alt*–TyHPMI)/P4VP and poly(S–*alt*–TyHPMI)/PVP binary blends shows the larger positive *q* value calculated based on the Kwei equation. Furthermore, one–dimensional (1D) and two–dimensional (2D) FTIR spectroscopy were employed to confirm the stronger intermolecular hydrogen bonding strength and to explore how external perturbations, such as temperature changes, affect the intermolecular interactions in these binary blends.

2. Experimental section

2.1. Materials

Ethyl acetate (EA), diethyl ether (Et_2O), tyramine (97 %), and chloroform were sourced from Acros Organics. Tetrahydrofuran (THF) and hexane were obtained from Sigma Aldrich. Maleic anhydride, styrene (99 %), PVP (M_n = 58,000 g/mol) were acquired from Alfa Aesar. Acetic acid (99.8 %) was supplied by Honeywell Research Chemicals. *N, N*–dimethylformamide (DMF) was acquired from J. T. Baker. Magnesium sulfate anhydrous ($MgSO_4$, 99 %) and azobisisobutyronitrile (AIBN) were purchased from SHOWA. All chemicals were used without further purification. The poly(S–*alt*–HPMI) and P4VP (M_n = 77,360 g/mol, PDI = 1.05) have been synthesized previously [30,31].

2.2. N-(ethyl-4-hydroxyphenyl)maleimide (TyHPMI)

Tyramine (4.06 g, 29.59 mmol) and maleic anhydride (3.48 g, 35.51 mmol) were placed into a 150 mL round–bottom flask. Subsequently, the addition of acetic acid (80 mL) was introduced, and the mixture was heated to 90 °C, resulting in a milky white solution. Once the solution became clear, it was further reflux for 16 h. After the solution cooled to room temperature, it was diluted with water and extracted four times with chloroform (4 × 200 mL). The collected chloroform layer was dried with $MgSO_4$ powder and then concentrated using a rotary evaporator. The purification of crude product was using flash chromatography for giving a pale yellow solid [35]. [Yield: 48 %; TLC: R_f = 0.44 (EA/hexane, 3/2)]; m.p. 146 °C (Fig. S1); FTIR (KBr, cm^{-1}): 3458 (O–H), 1704 (C=O); ^{1}H NMR (500 MHz, DMSO–d_6, δ, ppm): 2.68 (t, 2H, Ar–C**H$_2$**), 3.55 (t, 2H, Mal–C**H$_2$**) 6.63 (d, 2H, Ar–**H**), 6.92 (d, 2H, Ar–**H**), 6.95 (s, 2H, C**H**=C**H**), 9.22 (s, 1H, O**H**); ^{13}C NMR (125 MHz, DMSO–d_6, δ, ppm): 33.07 (**C**H$_2$–**C**H$_2$), 115.85, 128.88, 130.28 (Ar–**C**), 135.18 (**C**H=**C**H), 156.67 (**C**–OH), 171.80 (**C**=O).

2.3. Poly(S–alt–TyHPMI)

A 150 mL two–necked round–bottom flask containing TyHPMI (1.5 g, 6.9 mmol) and AIBN (5 wt%) was subjected to a vacuum/N_2 cycle. Dry THF (47 mL) was then injected to dissolve the solid. Subsequently, the mixture was stirred until clear, followed by the injection of styrene (0.72 g, 6.9 mmol). The mixture was then treated with three freeze–pump–thaw/N_2 cycles. The solution was heated to 70 °C and stirred under a nitrogen atmosphere for 24 h. The solution was exposed to air for an hour to terminate the reaction. The solvent was then removed using a rotary evaporator, and the concentrated solution was dropped into cold Et_2O to obtain precipitate. The solid was repeatedly reprecipitated to purify the product and then dried under reduced pressure at 40 °C for 4 days to remove any residual solvent. FTIR (KBr, cm^{-1}): 3449 (O–H), 1694 (C=O); ^{1}H NMR (500 MHz, DMSO–d_6, δ, ppm): 6.04–7.62 (m, 9H, Ar**H**), 9.22 (s, 1H, O**H**); ^{13}C NMR (125 MHz, DMSO–d_6, δ, ppm): 32.18 (TyHPMI–**C**H$_2$**C**H$_2$), 114.75–131.43 (Ar–**C**), 156.75 (**C**–OH), 176.86–179.90 (**C**=O); GPC was measured through DMF system (number–average molecular weight, M_n = 22,700 g/mol and polymer dispersity index (PDI) = 1.63) (Fig. S2).

2.4. Binary blends of poly(S–alt–TyHPMI) with P4VP or PVP

The solution–casting method was used to prepare the binary blends of poly(S–*alt*–TyHPMI) with P4VP or PVP with a 5 wt% polymer composition. These blends were dissolved in DMF and stirred overnight until a homogeneous solution was obtained. Afterward, the binary mixture was treated at 90 °C in a vacuum oven for one week to make sure any residual solvent was removed completely.

3. Results and discussion

3.1. TyHPMI monomer synthesis

The synthesis of TyHPMI monomer, as shown in Fig. 1(a), involved reacting maleic anhydride with tyramine under the acidic condition, generating a short alkyl chain that serves as the spacer between the phenolic OH and the maleimide group [35]. The FTIR spectrum in Fig. 1 (b) shows distinct sharp absorption signals at 3458 cm^{-1} and 1704 cm^{-1}, corresponding to the O–H and C=O stretching vibrations of TyHPMI monomer, respectively. The weak aliphatic C–H vibration signals at ca. 2948 cm^{-1} contributed to the alkyl units in TyHPMI monomer. In comparison, this signal is not observed in the FTIR spectra of HPMI, as shown in Fig. S3. Furthermore, the O–H and C=O signals of TyHPMI featured at lower wavenumbers compared with HPMI as illustrated in Figs. S3(b)–S3(c). The reduced wavenumber can be ascribed to the following factors: (1) compared to HPMI, the short alkyl chain on TyHPMI decreases the electron density around the phenolic OH and C=O groups, leading to a reduction in their dipole moments and a more stable state and (2) the short alkyl chains on TyHPMI also results in the formation of more resonance structures from the phenolic units [36].

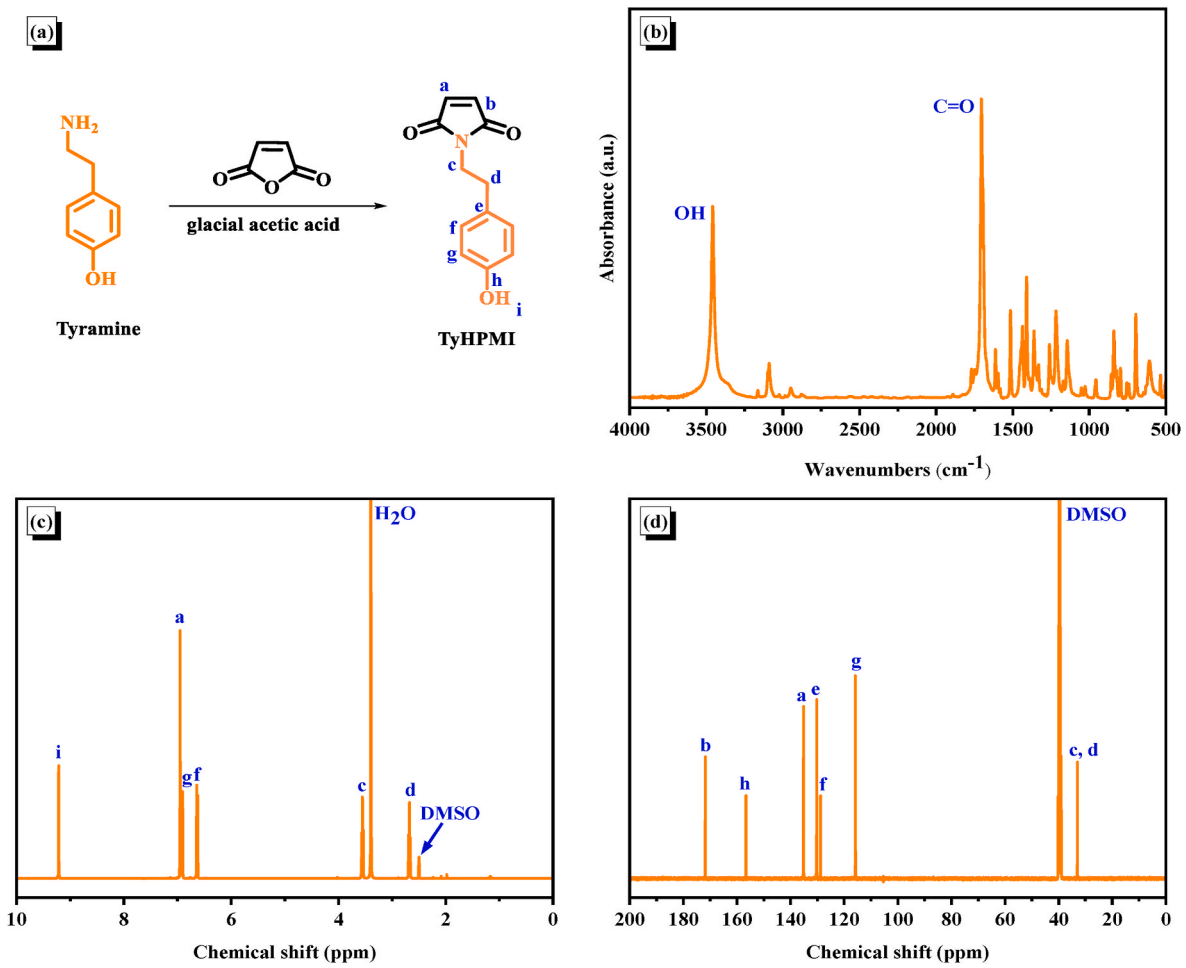

Fig. 1. (a) Synthesis of the TyHPMI monomer. (b) FTIR spectrum of TyHPMI monomer. (c) ^{1}H NMR spectrum of TyHPMI monomer. (d) ^{13}C NMR spectrum of TyHPMI monomer.

Additionally, the C=O signal of TyHPMI, as shown in Fig. S3(c), displayed a shoulder at 1697–1660 cm^{-1}, indicating intermolecular hydrogen bonding [27]. Fig. 1(c) displays the ^{1}H NMR spectrum of the TyHPMI monomer and the signals for the phenolic OH unit of TyHPMI appeared at 9.22 ppm, while the protons attached to the olefinic unit appeared at 6.95 ppm. Additionally, the signals for protons on the short alkyl chains appeared at 3.55 and 2.68 ppm, corresponding to their proximity to the maleimide and phenol groups, respectively [35]. ^{13}C NMR spectrum in Fig. 1(d) featured the carbon signals for the C=O, C–OH, olefinic units and alkyl carbon chains at 171.80, 156.67, 135.18 and 33.07 ppm, respectively [37]. These FTIR and NMR spectra results were confirmed the successful synthesis of the TyHPMI monomer.

3.2. Poly(S–*alt*–TyHPMI) synthesis

The synthesis of poly(S–*alt*–TyHPMI) alternating copolymer was conducted via free radical copolymerization of styrene and TyHPMI monomers, as depicted in Fig. 2(a). The chemical structures of poly (S–*alt*–TyHPMI) was confirmed by using FTIR and NMR spectroscopy. After removing the water from poly(S–*alt*–TyHPMI), the collected FTIR spectrum is shown in Fig. 2(b). The characteristic O–H and C=O signals appear at 3447 cm^{-1} and 1695 cm^{-1}, respectively. Compared with Fig. 1 (b), the O–H vibration signal of poly(S–*alt*–TyHPMI) was broader than that of the TyHPMI monomer, indicating the presence of hydrogen bonds between or within molecular chains after copolymerization with styrene. Additionally, DSC analysis as shown in Fig. S1 revealed that the melting point of the TyHPMI monomer at 146 °C transitioned to a single T_g value in poly(S–*alt*–TyHPMI) after copolymerization. Clearly, the T_g value of poly(S–*alt*–TyHPMI) was significantly lower than that of poly (S–*alt*–HPMI), with a value of 259 °C [27]. This reduction in T_g value may be attributed to the short alkyl units in the TyHPMI, which enhanced the flexibility and provided additional free volume [38]. Furthermore, compared to the O–H and C=O signals of poly (S–*alt*–HPMI) as illustrated in Fig. 2(c)-2(d), the signals of poly (S–*alt*–TyHPMI) exhibited narrower and appeared at lower wavenumbers. The results indicate that the stronger hydrogen bonding interaction between molecular chains in poly(S–*alt*–TyHPMI) [27]. ^{1}H NMR spectrum of poly(S–*alt*–TyHPMI) displayed in Fig. 2(e) showed characteristic signals for OH and aromatic protons appearing at 9.22 and 6.04–7.62 ppm, respectively. The ^{13}C NMR as displayed in Fig. 2(f) featured the signals for C=O at 176.86–179.90 ppm, Ph–OH at 156.75 ppm, the aromatic carbon units at 114.75–131.43 ppm, and the short alkyl chain units at 32.18 ppm. All these results were confirmed the successful synthesis of poly(S–*alt*–TyHPMI) copolymer.

To confirm the sequence distribution of poly(S–*alt*–TyHPMI) copolymer, we integrated the peaks of OH and aromatic rings in the proton NMR spectrum, representing the TyHPMI and styrene monomers, respectively. The ratio of TyHPMI to styrene was found to be 1:1.15, corresponding to the expected alternating copolymer. Additionally, we collected the MALDI–TOF mass spectrum, as shown in Fig. 3, to provide more convincing evidence for alternating sequence. The sum of TyHPMI units was almost equal to the sum of styrene units. For instance, the difference of two significant signals at *m/z* 2876.70 and 3198.08 was about 321 g mol^{-1}, which corresponds to a pair of TyHPMI and styrene

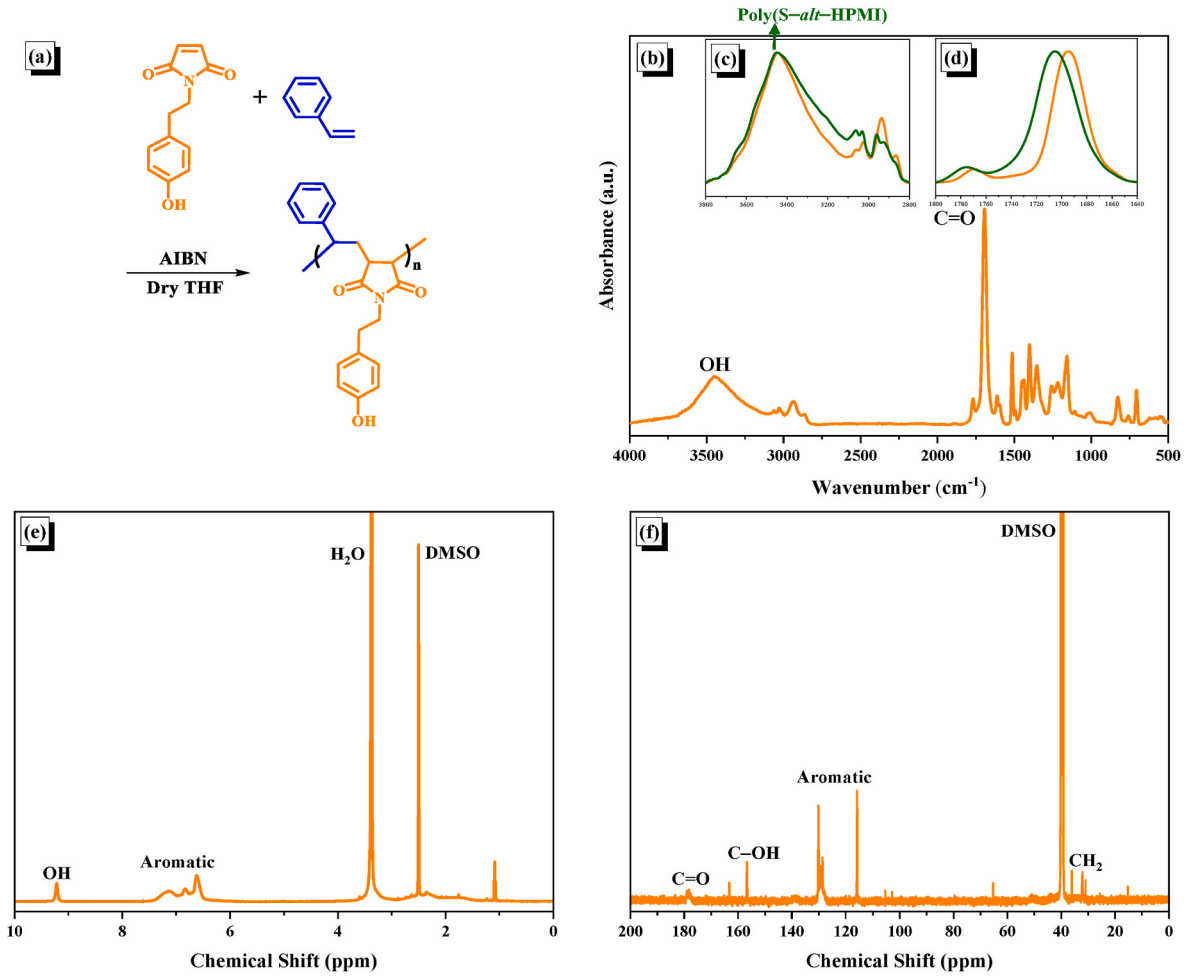

Fig. 2. (a) Synthetic scheme of poly(S–*alt*–TyHPMI). Fig. 2(b–d): FTIR spectra of poly(S–*alt*–TyHPMI): (b) full spectrum, (c) enlarged view of the OH group region with poly(S–*alt*–HPMI), and (d) enlarged view of the C=O group region with poly(S–*alt*–HPMI). (e) ^{1}H NMR spectrum of poly(S–*alt*–TyHPMI). (f) ^{13}C NMR spectrum of poly(S–*alt*–TyHPMI).

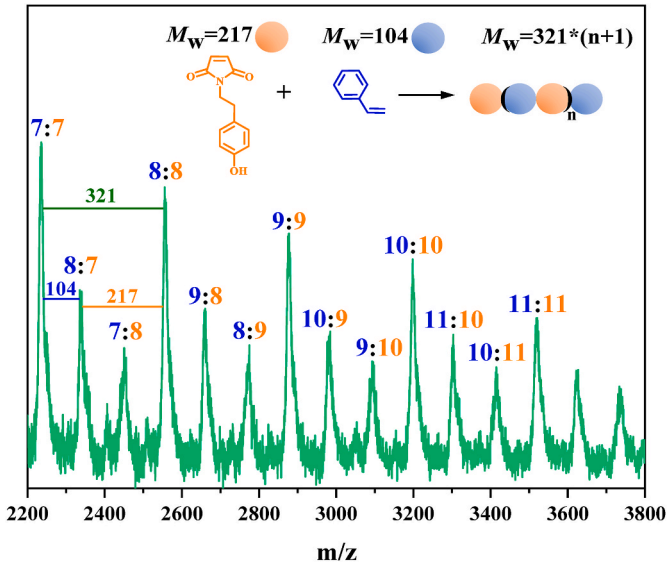

Fig. 3. MALDI-TOF mass spectrum of poly(S–*alt*–TyHPMI).

unit molecular weight. Moreover, the signal labeled "7:7" at *m/z* 2235.02 consist of 7 units of TyHPMI and 7 units of styrene. Other significant signals such as n:n, n+1: n, n: n+1 and n+1: n+1 (e.g., 7:7, 8:7, 7:8 and 8:8) represent perfect TyHPMI and styrene alternating sequences.

3.3. Analyses of poly(S–alt–TyHPMI)/P4VP blends

In this study, we selected the strong hydrogen bonded acceptor homopolymer with higher K_A value as PVP or P4VP homopolymer, which had strong inter–association and could result in a higher K_A/K_B ratio. Firstly, we blended P4VP with poly(S–*alt*–TyHPMI) in various weight fractions and recorded the DSC thermograms, as shown in Fig. 4(a). The pure P4VP and poly(S–*alt*–TyHPMI) exhibited T_g values of 131 °C and 146 °C, respectively. As mentioned in previous section, the T_g value of poly(S–*alt*–TyHPMI) was lower also compared to, poly(S–*alt*–oHPMI) (T_g = 249 °C) and poly(S–*alt*–DMHPMI) (T_g = 242 °C) [27,28], as well as styrene–maleic anhydride (T_g = 184 °C) [39] and styrene–*N*–phenylmaleimide (T_g = 196 °C) without introduced hydrogen bonded donor [40]. This reduction in T_g values can be attributed to the alkyl chains in TyHPMI units, which enhance the mobility of the polymer chain and decrease its rigidity. The increased mobility also results in a greater free volume, leading to the expected decrease in T_g value [38]. Remarkably, in each weight fraction of binary blend, only a single T_g value was observed and the most blending compositions are higher than the individually pure P4VP and poly(S–*alt*–TyHPMI), indicating that

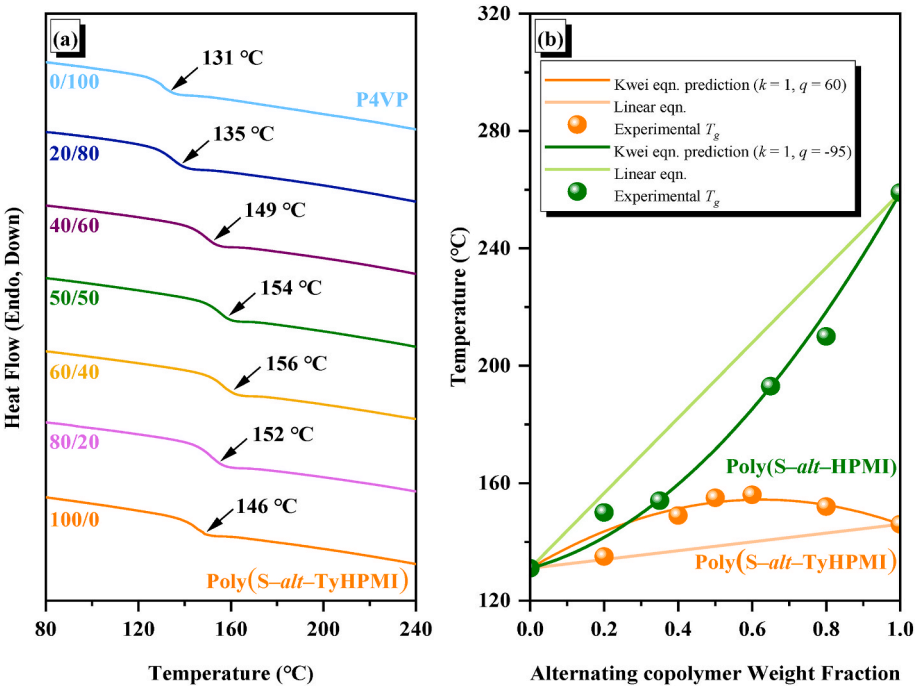

Fig. 4. (a) T_g values measured by DSC for blends of P4VP with poly(S–*alt*–TyHPMI) at diverse weight fractions. (b) Experimental T_g values, Kwei equation prediction and linear equation for blends of P4VP with poly(S–*alt*–TyHPMI) and compared to P4VP blends with poly(S–*alt*–HPMI).

poly(S–*alt*–TyHPMI)/P4VP binary blends are fully miscible and exhibit excellent miscibility. Furthermore, we fit the experimental T_g value based on Fig. 4(a) by utilizing the Kwei equation [29]. Fig. 4(b) illustrated the Kwei equation predictions for poly(S–*alt*–TyHPMI)/P4VP blends exhibit positive deviations from the linear rule for k and q values of 1 and 60, respectively. Interestingly, this contrasts with the results from our previous study of poly(S–*alt*–HPMI)/P4VP, which with values k and q of 1 and –95. This result can be attributed to the following factor:

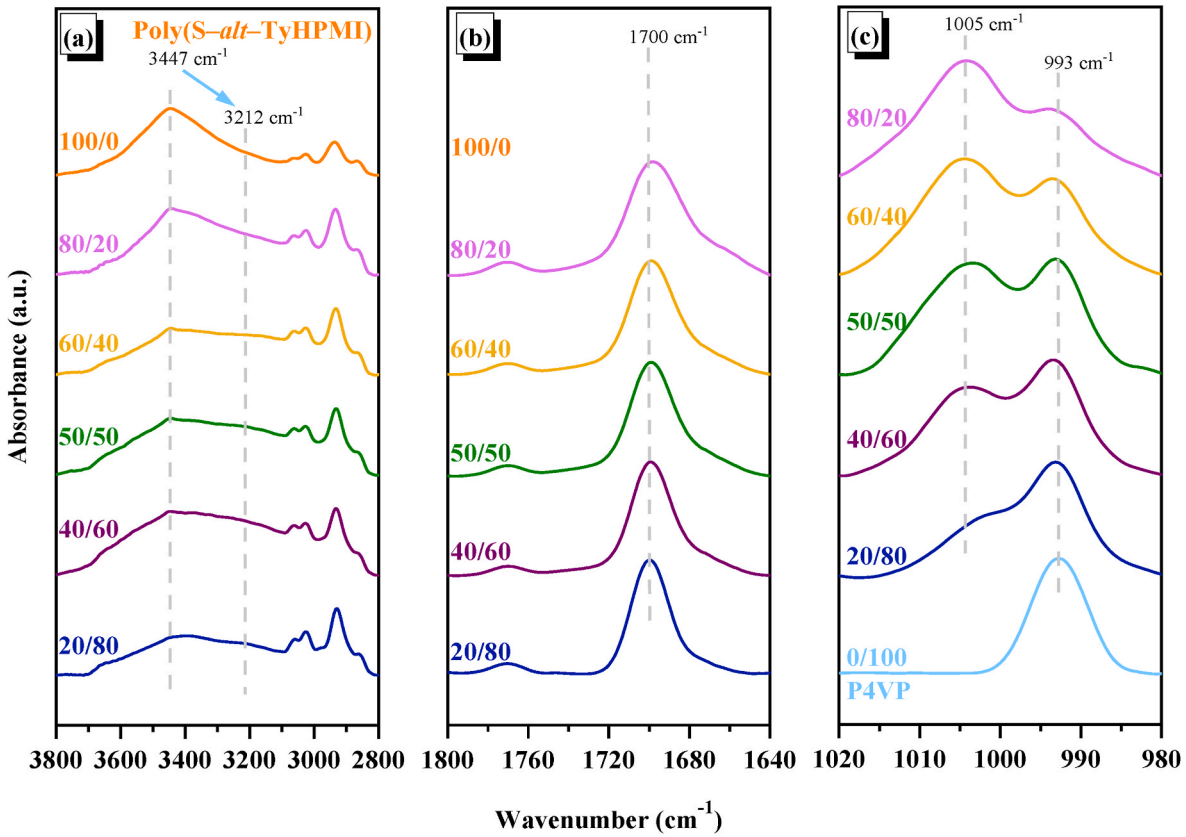

Fig. 5. FTIR spectra of blends of poly(S–*alt*–TyHPMI) with P4VP (a) hydroxyl group, (b) carbonyl group and (c) pyridyl group region.

(1) the OH and C=O groups of the HPMI unit in poly(S–*alt*–HPMI) interact closely within the molecule, leading to stronger intramolecular interactions and preventing the strengthening of intermolecular interactions [45]. and (2) the self–association hydrogen bonding of OH···OH and OH···O=C units of poly(S–*alt*–TyHPMI) was decreased, thereby reducing the K_B value and further increasing the K_A/K_B ratio in blend system [28]. In addition, the overlay plots of the Kwei equations for poly(S–*alt*–HPMI)/P4VP and poly(S–*alt*–TyHPMI)/P4VP indicated that the intersection point occurred at ca. 25 wt% of the alternating copolymer in the blend system. This demonstrates that less than this weight fraction, poly(S–*alt*–TyHPMI) can more effectively improve the thermal properties (similarly T_g behavior) when blending with P4VP even though the T_g value of pure poly(S–*alt*–TyHPMI) is much lower than pure poly(S–*alt*–HPMI).

To understand why the q value of poly(S–*alt*–TyHPMI)/P4VP becomes positive, differing from our previous report, we examined the hydrogen bonding interactions of this blend system using FTIR spectroscopy after removing moisture. Fig. 5(a) shows the O–H vibration signals of pure poly(S–*alt*–TyHPMI) at 3447 cm^{-1}, which include the OH···OH and OH···O=C self–associated hydrogen bonds. As the content of P4VP in the binary blend system was increased, the intensity of the O–H vibration signals decreased and shifted to 3212 cm^{-1}, indicating that the hydroxyl groups change to interact with N atoms in P4VP, forming OH···N inter–associated hydrogen bonding. Additionally, Fig. 5 (b) showed that as the proportion of P4VP in the blend increased, the C=O signals in poly(S–*alt*–TyHPMI) became narrower and shifted to higher wavenumbers at 1700 cm^{-1}, indicating the disruption or decreasing of OH···O=C self–associated hydrogen bonding. Furthermore, the hydrogen bonding attraction in P4VP was distinguished by the C–H bending signals of pyridyl groups, showed that pure P4VP exhibited free pyridyl groups at 993 cm^{-1}. As the proportion of poly (S–*alt*–TyHPMI) in the binary blending system increased, the signal intensity at 1005 cm^{-1} gradually increased, directing the formation of OH···N inter–associated hydrogen bonding.

On the other hand, we fitted the signals of pyridyl groups using Gaussian functions to clearly observe the changes in free and hydrogen–bonded pyridyl groups in a series of poly(S–*alt*–TyHPMI)/P4VP binary blends, as displayed in Fig. 6(a). Fig. 6(b) and Fig. S4 summarized the FWHMs of carbonyl signals and hydrogen–bonded N atoms in diverse weight fraction blends of P4VP with two kinds of alternating copolymers. The results clearly show that the fraction of hydrogen–bonded N atoms in P4VP blends with poly(S–*alt*–TyHPMI) were always higher than that in P4VP blends with poly(S–*alt*–HPMI); however, the width of C=O groups in P4VP blends with poly(S–*alt*–TyHPMI) were always lower. This indicated that poly(S–*alt*–TyHPMI) exhibited as a stronger intermolecular hydrogen bonding donor due to the introduction of the short alkyl unit, which enhances its ability to form the intermolecular hydrogen bonding with P4VP.

Furthermore, we also investigated the impact of external perturbation on hydrogen bonding in blends of P4VP with poly(S–*alt*–TyHPMI). The poly(S–*alt*–TyHPMI)/P4VP = 50/50 blend was chosen for analysis and measured using FTIR over a temperature range of 60–180 °C. Fig. 7 (a) and (b) displayed that the C=O groups signals showed slightly response to temperature changes, but the intensity of hydrogen–bonded pyridyl groups was significantly decreased with increasing temperature, indicating the predominant formation of OH···N inter–associated hydrogen bonding rather than OH···O=C self–associated hydrogen bonding. We further analyzed hydrogen–bonded behavior using 2D FTIR spectra, following the approach of Noda group, which not only enhanced spectral resolution but also allowed us to determine the sequence of changes in free and hydrogen–bonded pyridine rings [41, 42]. Fig. 7(c) characterize the synchronous 2D IR correlation map of pyridyl region at 980–1200 cm^{-1}. There were two susceptible signals located in the diagonal area near 993 cm^{-1} and 1005 cm^{-1}, representing free pyridine rings and hydrogen–bonded pyridine rings, respectively. The negative cross peak was located in the off–diagonal region at the intersection of 993 cm^{-1} and 1005 cm^{-1}, indicating that these two signals varied in opposite tendencies: as the free pyridine rings increase, the hydrogen–bonded pyridine rings decreased. Conspicuously, the asynchronous 2D correlogram depicted in Fig. 7(d) showed a positive cross peak appeared in the lower right corner (1005 vs. 993 cm^{-1}), in contrast to the synchronous correlogram in Fig. 7(c), which exhibited an opposite trend. Based on the Noda's rule, the signal at 1005 cm^{-1} induced by increasing temperature precedes the signal at 993 cm^{-1}. This

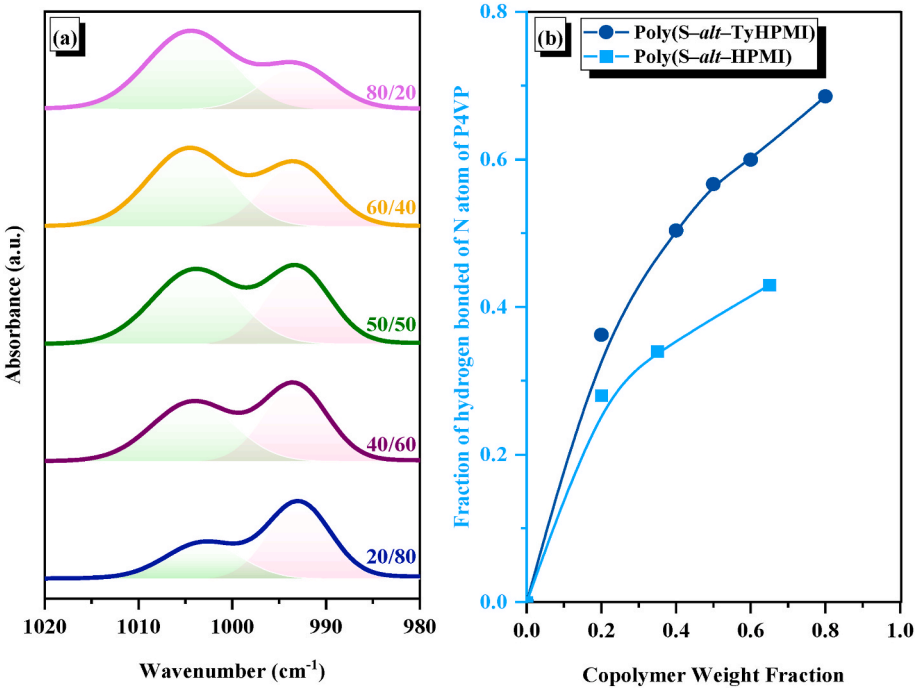

Fig. 6. (a) Curve fitting results from FTIR spectra of C–H bending of pyridyl group region for poly(S–*alt*–TyHPMI)/P4VP binary blends. (b) FWHMs of carbonyl signals and hydrogen–bonded N atoms in diverse weight fraction blends of P4VP with poly(S–*alt*–TyHPMI) compared with poly(S–*alt*–HPMI).

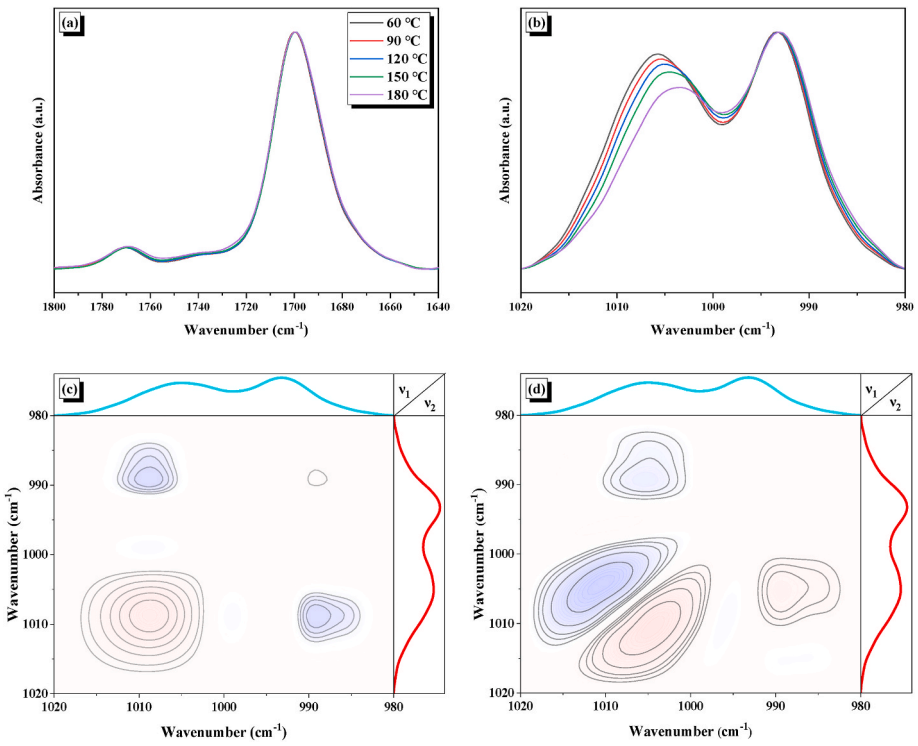

Fig. 7. (a, b) FTIR spectra in the blends of P4VP with poly(S–*alt*–TyHPMI) (a) C=O group region and (b) C–H bending of pyridyl group region, recorded from 60 to 180 °C, for the 50/50 ratio. (c, d) 2D FTIR spectra of C–H bending of pyridyl group region of (c) synchronous and (d) asynchronous correlation maps.

phenomenon was plausible because the hydrogen bonds between the OH groups in poly(S–*alt*–TyHPMI) and N atom in pyridine rings were sensitive to temperature changes. As the temperature increases, the OH···N inter–associated hydrogen bonds broke, resulting in the formation of free pyridine rings as expected.

3.4. Analyses of poly(S–alt–TyHPMI)/PVP blends

In this section, we interested in exploring the results of poly (S–*alt*–TyHPMI) blends with PVP, which has the highest K_A value when blended with PVPh [7]. Fig. 8(a) displays the DSC thermogram for various weight fractions of PVP blends with poly(S–*alt*–TyHPMI), each showing the individual T_g, indicating excellent miscibility of this blend

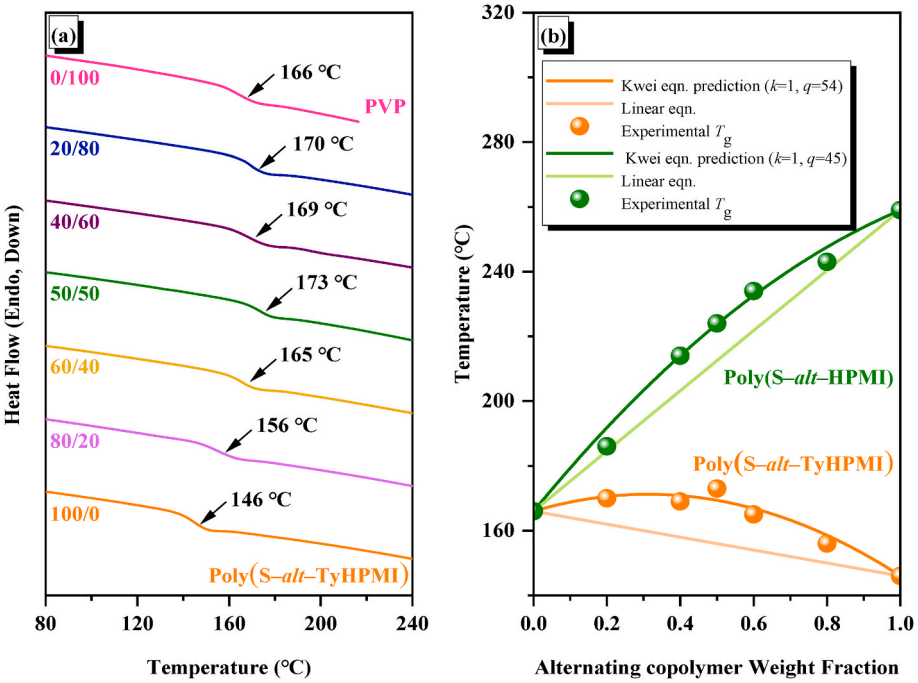

Fig. 8. (a) T_g values measured by DSC for blends of poly(S–*alt*–TyHPMI) with PVP at diverse weight fractions. (b) Experimental T_g values, Kwei equation prediction and linear equation in blends of PVP with poly(S–*alt*–TyHPMI) and compared to blends of PVP with poly(S–*alt*–HPMI).

system. Furthermore, we fit the experimental T_g by applying the Kwei equation, as demonstrated in Fig. 8(a). Fig. 8(b) presents the prediction of Kwei equation [29] for poly(S–*alt*–TyHPMI)/PVP blends, which exhibited a convex curve above the linear rule as expect, with values k and q of 1 and 54, respectively. On the other hand, the q value of PVP blends with poly(S–*alt*–TyHPMI) was higher than that of PVP blended with poly(S–*alt*–HPMI), indicating the stronger inter–associated hydrogen bonding within the PVP and poly(S–*alt*–TyHPMI).

To confirm the higher q value corresponds to stronger hydrogen bonding in blends of PVP with poly(S–*alt*–TyHPMI), we used FTIR spectroscopy to investigate the hydrogen bonding behaviors in the blends after completely removing moisture. Fig. 9(a) shows the O–H vibration signals of pure poly(S–*alt*–TyHPMI) at 3447 cm^{-1}, representing self–associated hydrogen bonds as mentioned in previous section. Followed the proportion of PVP in the binary blend increased, the intensity of the O–H vibration signals decreased and shifted to 3217 cm^{-1}. This shift suggests that the introduction of PVP, with its more competitive C=O hydrogen–bonded acceptors, converts the OH···OH and OH···O=C self–associated hydrogen bonds in pure poly(S–*alt*–TyHPMI) into OH···O=C inter–associated hydrogen bonds with PVP. We also investigated the variations of C=O signals shown in Fig. 9(b). The signal at 1680 cm^{-1} in PVP was identified as free C=O unit [43,44]. Upon introducing poly(S–*alt*–TyHPMI), this signal moved to 1660 cm^{-1} with a lower wavenumber, suggesting the formation of inter–associated OH···O=C bonds between poly(S–*alt*–TyHPMI) and PVP. Furthermore, followed the increase of PVP proportion in the binary blend system, the C=O signals in poly(S–*alt*–TyHPMI) shifted to higher wavenumbers at 1703 cm^{-1}, also indicating the disruption and decreasing of OH···O=C self–associated hydrogen bonding.

To quantify the amount of hydrogen–bonded PVP, we also fitted the C=O groups signals using Gaussian functions in a series of PVP blends with poly(S–*alt*–TyHPMI), as displayed in Fig. 10(a). Fig. 10(b) summarized the fraction of hydrogen–bonded C=O groups in two types of alternating copolymers blended with PVP at different weight fractions. The results clearly showed that the fraction in blends of PVP with poly (S–*alt*–TyHPMI) is consistently higher than those in blends of PVP with poly(S–*alt*–HPMI). This indicated that poly(S–*alt*–TyHPMI) act as a stronger hydrogen bonding donor due to the introduction of the alkyl units, which enhances its ability to form inter–associated hydrogen bonds. Finally, we also investigated the influence of temperature perturbation on poly(S–*alt*–TyHPMI)/PVP binary blends, considering the temperature sensitivity of hydrogen bonding.

A 50/50 wt fraction of poly(S–*alt*–TyHPMI)/PVP was selected for analysis and measured using FTIR over a temperature range of 60–180 °C. Fig. 11(a) and (b) displayed that the signals of O–H and C=O regions. The intensity around 3217 cm^{-1}, corresponding to hydroxyl groups, decreased as the temperature increased. However, the signals around 3447 cm^{-1} and in the C=O regions appeared to remain unchanged. To clearly distinguish these insignificant changes clearly, 2D IR spectroscopy was utilized again. Fig. 11(c) characterized the synchronous 2D IR correlation map of the O–H region versus the C=O region. It was evident that the signals around 3217 cm^{-1} exhibited significantly stronger correlation than those around 3447 cm^{-1}, indicating the predominant formation of OH···O=C inter–associated hydrogen bonds. Besides, the cross peak corresponding to C=O signals nearby 1660 cm^{-1}, 1680 cm^{-1} and 1703 cm^{-1} align with three susceptible signals located in the diagonal area displayed in Fig. 11(d), the synchronous 2D IR correlation map of C=O region at 1640–1740 cm^{-1}, verifying that these carbonyl groups were influenced by hydroxyl groups. Conspicuously, Fig. 11(c) showed positive cross peaks at (3217 cm^{-1} vs. 1703 cm^{-1}) and (3217 cm^{-1} vs.1660 cm^{-1}), indicating the self–associated OH···O=C in poly(S–*alt*–TyHPMI) and inter–associated OH···O=C with PVP, respectively. A negative cross peak at (3217 cm^{-1} vs. 1680 cm^{-1}), representing the free C=O, is reasonable because the inter–associated OH···O=C formation coincides with a reduction in free C=O. According to the Noda's rule, the sequence of changes in tensity, as determined by the synchronous and asynchronous 2D correlogram (Fig. 11(d) and Fig. S5), upon increasing temperature followed the order: inter–associated OH···O=C (1660 cm^{-1}) > free O=C (1680 cm^{-1}) > self–associated OH···O=C (1703 cm^{-1}). This phenomenon determined that the construction of inter–associated hydrogen bonds were predominant and temperature–sensitive in blends of PVP with poly (S–*alt*–TyHPMI). As the temperature increases, the OH···O=C inter–associated hydrogen bonds broke, resulting in the formation of free

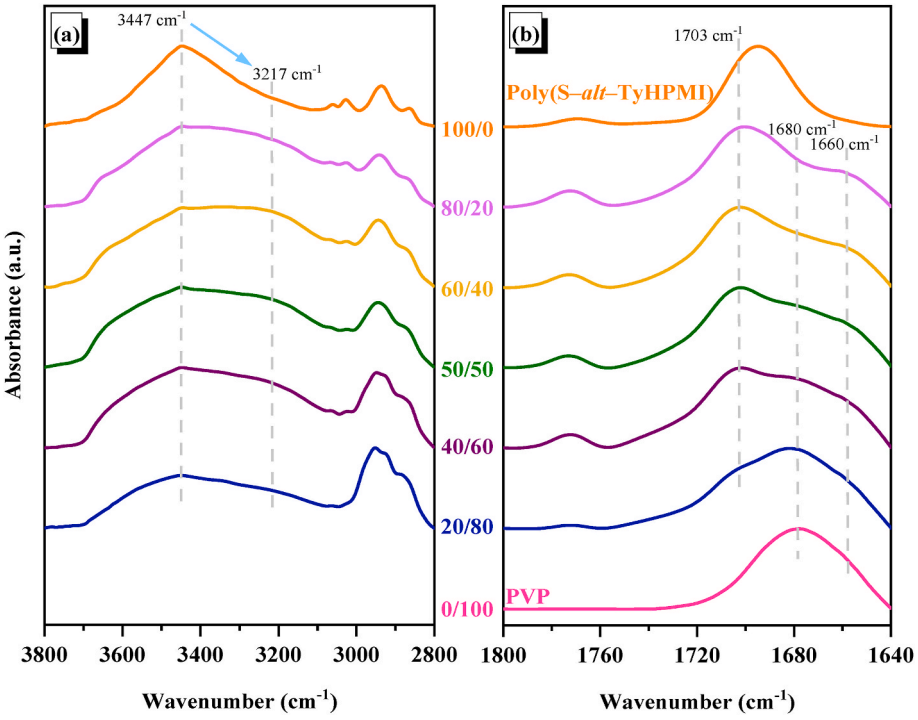

Fig. 9. FTIR spectra of blends of poly(S–*alt*–TyHPMI) with PVP (a) hydroxyl group, (b) carbonyl group.

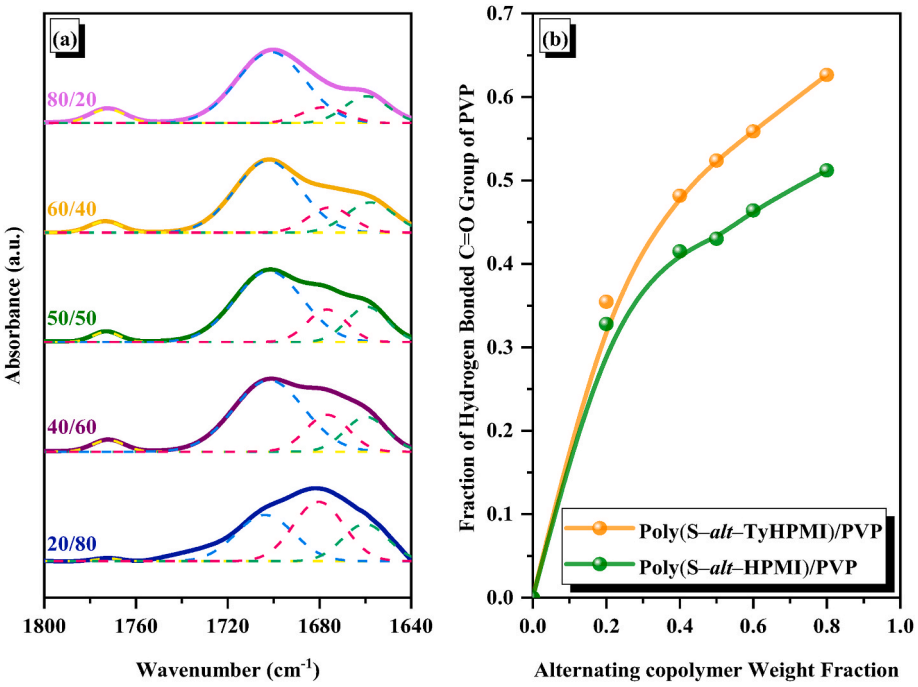

Fig. 10. (a) Curve fitting results from FTIR spectra of C=O group region for blends of PVP with poly(S–*alt*–TyHPMI). (b) Fraction of C=O group in diverse weight fraction blends of PVP with poly(S–*alt*–TyHPMI) compared with poly(S–*alt*–HPMI).

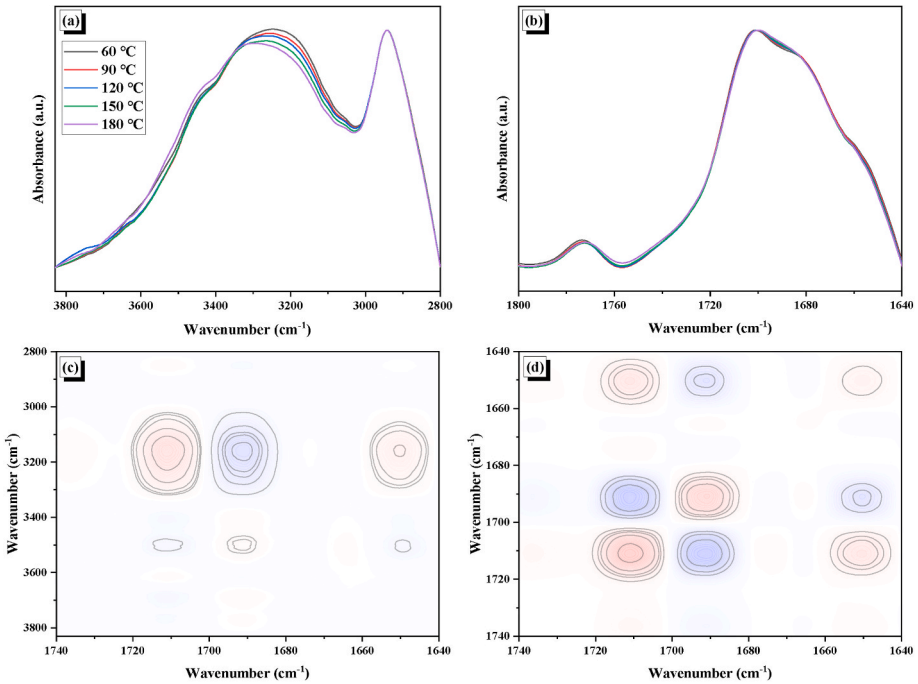

Fig. 11. (a, b) FTIR spectra in the blends of PVP with poly(S–*alt*–TyHPMI) (a) hydroxyl group region and (b) carbonyl group region, recorded from 60 to 180 °C, for the 50/50 ratio. (c, d) 2D FTIR spectral synchronous correlation maps of (c) O–H group stretching vs. C=O group region. (d) C=O group region.

PVP. However, the last sequence of self–associated OH···O=C in pristine poly(S–*alt*–TyHPMI) may due to the low quantity, resulting in a less sensitive temperature response.

4. Conclusions

We synthesized the TyHPMI monomer and then employed it to react with styrene, forming poly(S–*alt*–TyHPMI) alternating copolymers via free radical copolymerization. The chemical structures were confirmed using FTIR and NMR spectroscopy. The MALDI–TOF mass spectrometry provided the evidence of the alternating sequence in poly (S–*alt*–TyHPMI). A distinct T_g value measured by DSC for each weight fraction of poly(S–*alt*–TyHPMI)/P4VP and poly(S–*alt*–TyHPMI)/PVP binary blends, indicating full miscibility without macrophase separation. A convex curve above the linear rule in the T_g behavior in the blends of P4VP with poly(S–*alt*–TyHPMI), different from the results of

blending with poly(S–*alt*–HPMI), suggested that the short alkyl chain enhances the acidity of TyHPMI units and strengthens intermolecular interactions. This was corroborated by curve fitting results of FTIR spectra, which summarized the proportion of hydrogen–bonded pyridyl and C=O groups. Similar results were observed in the blends of PVP with poly(S–*alt*–TyHPMI). 2D–FTIR was utilized to explore how external temperature perturbations affect the hydrogen–bond formation of pyridyl and C=O groups and to determine the sequence of changes among them. Overall, this study provides the simple design the chemical structure to suppress the self–associated OH···O=C group of HPMI segment by attaching two short carbon units, which enhances its ability to form the intermolecular hydrogen bonding with other hydrogen bonded acceptors.

Data availability

The data that has been used is confidential.

CRediT authorship contribution statement

Tzu-Ling Ma: Writing – original draft, Formal analysis, Data curation. **Wei-Ting Du:** Writing – original draft, Formal analysis, Data curation, Conceptualization. **Shiao-Wei Kuo:** Writing – review & editing, Supervision, Resources, Funding acquisition, Conceptualization.

Declaration of competing interest

The authors declare that they have no known competing financial interests or personal relationships that could have appeared to influence the work reported in this paper.

Acknowledgments

This study was supported financially by the National Science and Technology Council, Taiwan, under contracts NSTC 113-2223-E-110-001- and 113-2221-E-110-012-MY3.

Appendix A. Supplementary data

Supplementary data to this article can be found online at https://doi.org/10.1016/j.polymer.2024.127574.

References

[1] F. Feng, J. Wu, C.Z. Liang, M. Weber, S. Zhang, T.S. Chung, Synergistic dual-polymer blend membranes with molecularly mixed macrocyclic cavitands for efficient pre-combustion CO2 capture, Chem. Eng. J. 470 (2023) 144073, https://doi.org/10.1016/j.cej.2023.144073.
[2] R. Ma, H. Li, T.A.D. Pena, X. Xie, P.W.K. Fong, Q. Wei, C. Yan, J. Wu, P. Cheng, M. Li, G. Li, Tunable donor aggregation dominance in a ternary matrix of all-polymer blends with improved efficiency and stability, Adv. Mater. 36 (2024) 2304632, https://doi.org/10.1002/adma.202304632.
[3] R.S. Chen, S. Ahmad, Mechanical performance and flame retardancy of rice husk/organoclay-reinforced blend of recycled plastics, Mater. Chem. Phys. 198 (2017) 57–65, https://doi.org/10.1016/j.matchemphys.2017.05.054.
[4] J. Feng, G. Zhang, K. MacInnis, Z. Li, A. Olah, E. Baer, Effect of compatibilizer on morphology and properties of HDPE/Nylon 6 blends, J. Polym. Sci., Part B: Polym. Phys. 57 (2019) 281–290, https://doi.org/10.1002/polb.24783.
[5] H.C. Zhang, B.H. Kang, L.S. Chen, X. Lu, Enhancing toughness of poly (lactic acid)/Thermoplastic polyurethane blends via increasing interface compatibility by polyurethane elastomer prepolymer and its toughening mechanism, Polym. Test. 87 (2020) 106521, https://doi.org/10.1016/j.polymertesting.2020.106521.
[6] M.M. Coleman, P.C. Painter, Hydrogen bonded polymer blends, Prog. Polym. Sci. 20 (1995) 1–59, https://doi.org/10.1016/0079–6700(94)00038–4.
[7] S.W. Kuo, Hydrogen Bonding in Polymeric Materials, John Wiley & Sons, Hoboken, NJ, USA, 2018. ISBN: 978–3–527–80426–9.
[8] S.W. Kuo, Hydrogen-bonding in polymer blends, J. Polym. Res. 15 (2008) 459–486, https://doi.org/10.1007/s10965-008-9192-4.
[9] C.L. Lin, W.C. Chen, C.S. Liao, Y.C. Su, C.F. Huang, S.W. Kuo, F.C. Chang, Sequence distribution and polydispersity index affect the hydrogen–bonding strength of poly (vinylphenol–co–methyl methacrylate) copolymers, Macromolecules 38 (2005) 6435–6444, https://doi.org/10.1021/ma050639t.
[10] S.W. Kuo, C.L. Lin, F.C. Chang, The study of hydrogen bonding and miscibility in poly (vinylpyridines) with phenolic resin, Polymer 43 (2002) 3943–3949, https://doi.org/10.1016/S0032–3861(02)00214–8.
[11] Y. He, B. Zhu, Y. Inoue, Hydrogen bonds in polymer blends, Prog. Polym. Sci. 29 (2004) 1021–1051, https://doi.org/10.1016/j.progpolymsci.2004.07.002.
[12] S.W. Kuo, P.H. Tung, F.C. Chang, Syntheses and the study of strongly hydrogen-bonded poly (vinylphenol-b-vinylpyridine) diblock copolymer through anionic polymerization, Macromolecules 39 (2006) 9388–9395, https://doi.org/10.1021/ma061713q.
[13] J.R. Isasi, C.L. Cesteros, I. Katime, Hydrogen bonding and sequence distribution in poly(vinyl acetate-Co-vinyl alcohol) copolymers, Macromolecules 27 (1994) 2200–2205, https://doi.org/10.1021/ma00086a033.
[14] J.G. Li, C.Y. Chung, S.W. Kuo, Transformations and enhanced long–range ordering of mesoporous phenolic resin templated by poly (ethylene oxide–b–ε–caprolactone) block copolymers blended with star poly (ethylene oxide)–functionalized silsesquioxane (POSS), J. Mater. Chem. 22 (2012) 18583–18595, https://doi.org/10.1039/C2JM33614F.
[15] C.C. Liu, W.C. Chu, J.G. Li, S.W. Kuo, Mediated competitive hydrogen bonding form mesoporous phenolic resins templated by Poly (ethylene oxide–b–ε–caprolactone–b–l–lactide) triblock copolymers, Macromolecules 47 (2014) 6389–6400, https://doi.org/10.1021/ma501246j.
[16] T.C. Chou, S.W. Kuo, Controllable wet-brush blending of linear diblock copolymers with phenolic/DDSQ hybrids toward mesoporous structure phase diagram, Macromolecules (2024), https://doi.org/10.1021/acs.macromol.4c00665.
[17] Y.C. Huang, W.C. Chen, S.W. Kuo, Mesoporous phenolic/POSS hybrids induced by microphase separation arising from competitive hydrogen bonding interactions, Macromolecules 55 (2022) 8918–8930, https://doi.org/10.1021/acs.macromol.2c01585.
[18] W.C. Chen, Y.T. Liu, S.W. Kuo, Mesoporous organic/inorganic hybrid materials with frank-kasper phases templated by an unusual linear symmetry diblock copolymer, Macromol. Rapid Commun. 42 (2021) 2100302, https://doi.org/10.1002/marc.202100302.
[19] M.G. Mohamed, E.C. Atayde Jr., B.M. Matsagar, J. Na, Y. Yamauchi, K.C.W. Wu, S. W. Kuo, Construction hierarchically mesoporous/microporous materials based on block copolymer and covalent organic framework, J. Taiwan Intst. Chem. Eng. 112 (2020) 180–192, https://doi.org/10.1016/j.jtice.2020.06.013.
[20] S.W. Kuo, Hydrogen bonding mediated self–assembled structures from block copolymer mixtures to mesoporous materials, Polym. Int. 71 (2022) 393–410, https://doi.org/10.1002/pi.6264.
[21] S.W. Kuo, Hydrogen bond-mediated self-assembly and supramolecular structures of diblock copolymer mixtures, Polym. Int. 58 (2009) 455–464, https://doi.org/10.1002/pi.2513.
[22] J.G. Li, P.Y. Lee, M.M. Ahmed, M.G. Mohamed, S.W. Kuo, Varying the hydrogen bonding strength in phenolic/PEO–b–PLA blends provides mesoporous carbons having large accessible pores suitable for energy storage, Macromol. Chem. Phys. 221 (2020) 2000040, https://doi.org/10.1002/macp.202000040.
[23] W.T. Du, S.Y. Chen, S.W. Kuo, Mesoporous phenolic/carbon materials templated by CO2-based PEO-b-PCHC diblock copolymers through mediated competitive intermolecular hydrogen bonding interactions for CO2 capture, J. CO_2 Util. 80 (2024) 102702, https://doi.org/10.1016/j.jcou.2024.102702.
[24] S.W. Kuo, Construction Archimedean tiling patterns based on soft materials from block copolymers and covalent organic frameworks, Giant 15 (2023) 100170, https://doi.org/10.1016/j.giant.2023.100170.
[25] A.F.M. EL-Mahdy, T.C. Yu, S.W. Kuo, Synthesis of multiple heteroatom–doped mesoporous carbon/silica composites for supercapacitors, Chem. Eng. J. 414 (2021) 128796, https://doi.org/10.1016/j.cej.2021.128796.
[26] S. Bag, S. Ghosh, S. Paul, M.E.H. Khan, P. De, Styrene–maleimide/maleic anhydride alternating copolymers: recent advances and future perspectives, Macromol. Rapid Commun. 42 (2021) 2100501, https://doi.org/10.1002/marc.202100501.
[27] W.T. Du, E.A. Orabi, M.G. Mohamed, S.W. Kuo, Inter/intramolecular hydrogen bonding mediate miscible blend formation between near-perfect alternating Poly (styrene-alt-hydroxyphenylmaleimide) copolymers and Poly (vinyl pyrrolidone), Polymer 219 (2021) 123542, https://doi.org/10.1016/j.polymer.2021.123542.
[28] W.T. Du, T.L. Ma, S.W. Kuo, Steric hindrance affects interactions of poly (styrene–alt–DMHPMI) copolymer with strongly hydrogen-bond-accepting homopolymers, Polymer 268 (2023) 125694, https://doi.org/10.1016/j.polymer.2023.125694.
[29] T. Kwei, The effect of hydrogen bonding on the glass transition temperatures of polymer mixtures, J. Polym. Sci. Polym. Lett. Ed. 22 (1984) 307–313, https://doi.org/10.1002/pol.1984.130220603.
[30] T.L. Ma, W.T. Du, S.W. Kuo, Construction of micelles and hollow spheres via the self-assembly behavior of poly (styrene-alt-pHPMI) copolymers with poly (4-vinylpyridine) derivatives mediated by hydrogen bonding interactions, Soft Matter 19 (2023) 4706–4716, https://doi.org/10.1039/D3SM00595J.
[31] T.L. Ma, W.T. Du, M.G. Mohamed, S.W. Kuo, Luminescent hollow spherical nanoparticles with enhanced imaging contrast through hydrogen bonding connected micelles, Eur. Polym. J. 210 (2024) 112954, https://doi.org/10.1016/j.eurpolymj.2024.112954.
[32] M. Chen, X. He, Y. Guo, J. Hu, B. Liang, K. Zeng, G. Yang, A new molecular design platform for high-performance polymers from versatile bio-based tyramine: a case study of tyramine-derived phthalonitrile resin, Polym. Chem. 12 (2021) 408–422, https://doi.org/10.1039/D0PY01322F.
[33] Y. Yang, Y. Lu, K. Zhang, A highly thermally stable benzoxazine resin derived from norbornene and natural renewable tyramine and furfurylamine, Eur. Polym. J. 187 (2023) 111895, https://doi.org/10.1016/j.eurpolymj.2023.111895.

[34] Q. Chen, D. Ren, W. Sheng, K. Zhang, Synthesis, polymerization and thermal properties of bio-based benzoxazine resins containing imide or amide functionality, J. Appl. Polym. Sci. 141 (2024) e54792, https://doi.org/10.1002/app.54792.
[35] L. Delafresnaye, C.W. Schmitt, L. Barner, C. Barner-Kowollik, A photochemical ligation system enabling solid-phase chemiluminescence read-out, Chem. Eur J. 25 (2019) 12538–12544, https://doi.org/10.1002/chem.201901858.
[36] W.T. Du, S.W. Kuo, Tunable thermal property of poly (styrene-alt-phenylmaleimide)-based alternating copolymers through mediated hydrogen bonding strength, Polymer 285 (2023) 126382, https://doi.org/10.1016/j.polymer.2023.126382.
[37] A. Presser, G. Lainer, N. Kretschmer, W. Schuehly, R. Saf, M. Kaiser, M.M. Kalt, Synthesis of jacaranone-derived nitrogenous cyclohexadienones and their antiproliferative and antiprotozoal activities, Molecules 23 (2018) 2902, https://doi.org/10.3390/molecules23112902.
[38] L.H. Sperling, Introduction to Physical Polymer Science, John Wiley & Sons., 2005. ISBN: 9780471706069.
[39] J.J. Benvenuta-Tapia, E. Vivaldo-Lima, J.A. Tenorio-López, M. Vargas-Hernández, H. Vázquez-Torres, Kinetic analysis of the RAFT copolymerization of styrene and maleic anhydride by differential scanning calorimetry, Thermochim. Acta 667 (2018) 93–101, https://doi.org/10.1016/j.tca.2018.07.013.
[40] Y. Liu, M. He, D. Zhang, Q. Zhao, Y. Li, S. Qin, J. Yu, P (N-Phenylmaleimide-Alt-Styrene) introduced with 4-carboxyl and its effect on the heat deflection temperature of nylon 6, Materials 11 (2018) 2330, https://doi.org/10.3390/ma11112330.
[41] I. Noda, Y. Ozaki, Two-dimensional Correlation Spectroscopy: Applications in Vibrational and Optical Spectroscopy, John Wiley & Sons, 2005. ISBN: 0-471-62391-1.
[42] K. Gong, L. Hou, P. Wu, Hydrogen-bonding affords sustainable plastics with ultrahigh robustness and water-assisted arbitrarily shape engineering, Adv. Mater. 34 (2022) 2201065, https://doi.org/10.1002/adma.202201065.
[43] S.W. Kuo, F.C. Chang, Studies of miscibility behavior and hydrogen bonding in blends of poly (vinylphenol) and poly (vinylpyrrolidone), Macromolecules 34 (2001) 5224–5228, https://doi.org/10.1021/ma010517a.
[44] W.C. Chen, S.W. Kuo, U.S. Jeng, F.C. Chang, Self-assembly through competitive interactions of miscible diblock copolymer/homopolymer blends: poly (vinylphenol-b-methyl methacrylate)/poly (vinylpyrrolidone) blend, Macromolecules 41 (2008) 1401–1410, https://doi.org/10.1021/ma7021925.
[45] M.G. Barlow, L. Sibous, A.E. Tipping, Intramolecular Diels-Alder reactions from trichloro-1, 2, 4-triazine and 1, 5-and 1, 6-dienes, Tetrahedron Lett. 33 (1992) 4653–4656, https://doi.org/10.1016/S0040-4039(00)61337-0.